DSC ANALYSIS OF ND-FE-B RIBBONS PREPARED BY MELT-SPINNING METHOD WITH DIVERSE COMPOSITIONS AND COOLING RATES

R. SABBAGHIZADEH[a*], R. SHAMSUDIN[a], N. DEYHIMIHAGHIGHI[b], A. SEDGHI[c]

[a]*Physics Department, Faculty of Science and Technology, National University of Malaysia, 43600 Bangi, Selangor, Malaysia*
[b]*Physics Department, Faculty of Science and Technology, University Putra Malaysia, 43400 UPM Serdang, Selangor, Malaysia*
[c]*Materials engineering, Faculty of Engineering and Technology, Qazvin, IRAN*

$Nd_{9.4}Pr_{0.6}Fe_{77.5-x}B_6Co_6Ga_{0.5}Ti_xC_x$ (x= 0, 1.5, 3, 4.5, 6) Melt-spun ribbons have been prepared at 15, 20 and 25 m/s quenching wheel speeds and were examined by using differential scanning calorimetry (DSC). It is remarkable that peak intensity increases with increasing solidification rate or the higher the Ti and C content of the structure. In both cases, the increased amounts of amorphous phase indicate their strongest peaks in the diagram. Another point related to the crystallization temperature of the ribbons in the presence of Ti and C, which will be discussed in detail in this manuscript.

1. Introduction

Rare Earth-Fe binary alloys have been substantially studied within the last decades mostly because of the higher coercivity obtained in as-cast bulk alloys and plus the significant role they play in governing the magnetic properties of Nd–Fe–B permanent magnets [1, 2]. Neodymium–iron–boron (Nd–Fe–B) magnets with prominent magnetic properties have been generated either via comminuted rapidly solidified melt-spun ribbons, as bonded or hot-formed magnets, or by sintering following prior green compaction in the applied magnetic field [3–5]. The main advantage of using the rapid quenching (R/Q) technology for acquiring high coercive Nd–Fe–B magnets reflects the possibility to effect through the cooling rate speed directly on the grain size and microstructure aimed at achieving magnetic microstructure which provides maximal magnetic energy of finished magnetic materials of this type [6–9]. Numerous studies have been made to improve the magnetic properties of Nd–Fe–B alloys by elemental substitution or rapid solidification processing techniques [10]. The crystallization evolution of the alloys is the investigation means of Differential Scanning Calorimetry (DSC). Differential scanning calorimetry is the main thermal-analysis method which combines the ease of measurement of heating and cooling curves with the quantitative features of calorimetry [11]. Crystallization is an incredibly sophisticated phenomenon, which highly depends on static and dynamic parameters included the process in. Different values purchased for the crystallization temperature (T_x) of the amorphous samples made by various techniques and having the identical composition reveal the formation of different amorphous structures or just the occurrence of the impurities. In close proximity to T_x most of the physical properties of the amorphous material, including magnetic ones, are changing considerably. Therefore the value of T_x ought to be known very correctly specifically for those amorphous materials used in applications. One of the main factors that influence the glass-forming ability of one metallic alloy is the thermal stability of the super-cooled

---

*Corresponding author: sabba@ukm.edu.my

liquid region (ΔT_x), defined as the region between glass-transition temperature (T_g) and crystallization temperature (T_x). This is dependent to the cooling rate and consequently to the preparation method. Previous studies have demonstrated that two factors determine the glass-forming ability: the magnitude of the super-cooled liquid region ($\Delta T_x = T_x - T_g$) and the value of the reduced glass-transition temperature (T_g / T_m, where T_m is the melting temperature). In subsequent studies, data about glass transition temperature (T_g) liquid region and the evolution of the crystallization process with the composition and samples thickness were acquired from calorimetric measurements (DSC) performed at a heating rate of 20 K/s. The difference between Fe-based and Nd-Fe-based amorphous alloys consists of the position of the glass-transition temperature relative to the crystallization temperature. For Fe-based, T_g is situated below T_x, and like in most of the previous studied amorphous alloys, for Nd-Fe-based T_g cannot be evidenced on DSC curves, because it is between T_x and T_m and the large glass-forming ability is given by the reduced crystallization temperature (T_x / T_m)[12].

2. Experimental procedure

Alloy ingots with nominal compositions of $Nd_{9.4}Pr_{0.6}$ $Fe_{77.5-x}B_6Co_6Ga_{0.5}Ti_xC_x$(a) x=0, (b) x= 1.5, (c) x=3, (e) x= 4.5 and (f) x= 6 were prepared from Fe, Nd, and Ti metals with purity greater than 99.5% and commercial-grade Fe–B and Fe–C alloys by induction melting in an argon gas atmosphere and casting onto a chilled hearth. The ingots were remelted four times in order to get the homogeneity. Ribbons were prepared from small pieces of crushed ingots by the single-roller melt-spinning technique at different wheel surface velocities (15, 20 and25 m/s) in an argon gas atmosphere. The chamber Ar pressure was 930mbar and the ejection pressure was 0.3 bars, and the orifice diameter of quartz tube was 0.5mm. The thickness of the as-spun ribbons (80–180 mm) decreased with wheel speed, confirming a steady increase of the cooling rate with increase of the wheel speed. The thermal analysis of the ribbons was carried out using a SETARAM DSC111 differential scanning calorimeter to determine the crystallization temperature.

3. Results and Discussion

Fig. *1* and

Fig. *2* show the DSC results of $Nd_{9.4}Pr_{0.6}$ $Fe_{77.5-x}B_6Co_6Ga_{0.5}Ti_xC_x$ (a) x=0, (b) x= 1.5, (c) x=3, (e) x= 4.5 and (f) x= 6 ribbons respectively, at different wheel speeds.

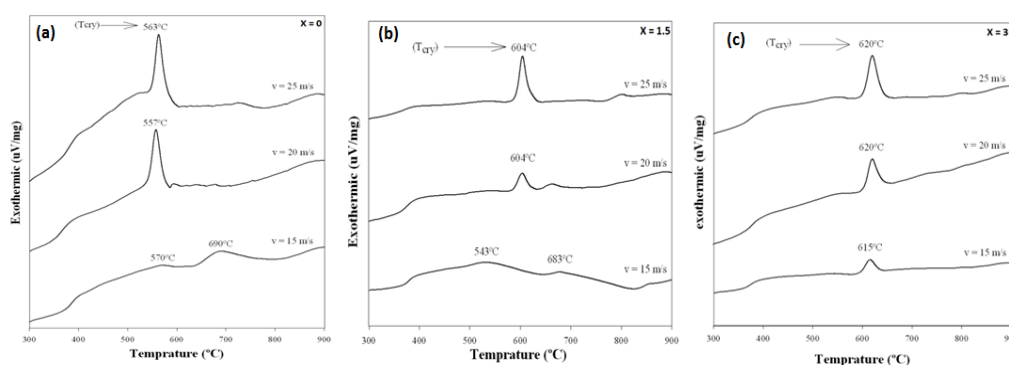*Fig. 1 DSC results of $Nd_{9.4}Pr_{0.6}$ $Fe_{77.5-x}B_6Co_6Ga_{0.5}Ti_xC_x$ (a) x=0, (b) x= 1.5 and (c) x=3*

All phase transformations that might occur during heating of the as-spun ribbons absorb or release energy; as a result, this transformation is exothermic or endothermic with peaks shown in their DSC curves. But, the dominant transformation of the as-spun ribbons is into their amorphous

part which released a lot of energy; as a result, the exothermic peak in the DSC curve is characterized.
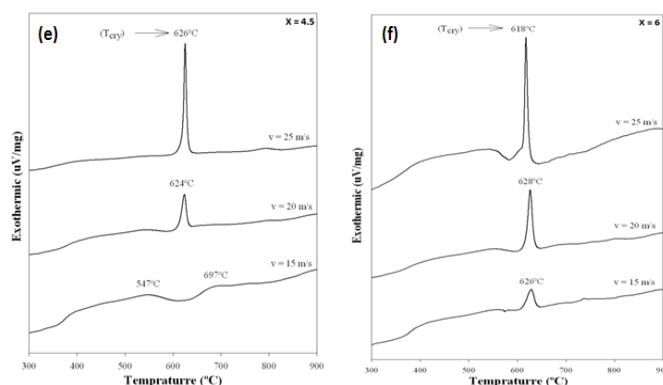

Fig. 2 DSC results of $Nd_{9.4}Pr_{0.6}Fe_{77.5-x}B_6Co_6Ga_{0.5}Ti_xC_x$ (e) x= 4.5 and (f) x= 6

Fig. 3 shows the DSC curves of the ribbons with different compositions based on the specified solidification rate. An overview of the DSC diagrams of the ribbons with different compositions and cooling rates shows the straight relation between peak intensity and solidification rate or Ti and C content of the structure. In both cases, the increased amounts of the amorphous phase indicate their strongest peaks in the diagram. Comparison of the DSC curves reveals that the main crystallization peak of the amorphous phase cannot be observed in (a) x= 0, (b) x= 1.5 and (e) x= 4.5 ribbons at 15 m/s, but for the other compounds and rates, the crystallization process of the amorphous phase has appeared with the sharp peak. The results show the high crystallinity structure of the aforementioned ribbons. It is practically impossible to ensure the final microstructure of the ribbons, but it is clear that the amount of the amorphous phase in the ribbons was so low that the energy of crystallization of the amorphous structure was not detected by the calorimeter.
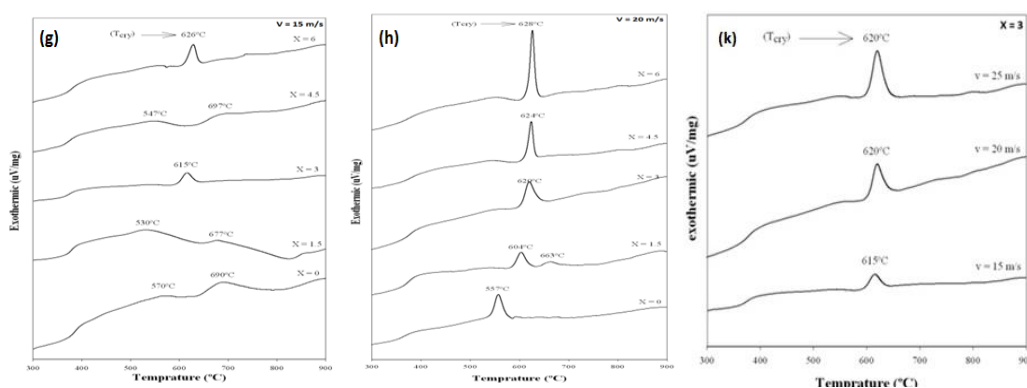

Fig. 3 DSC curves of the ribbons with different compositions based on the cooling Rate (g) v= 15, (h) x= 20and (k) x= 25 m/s

Fig. 4 and
Fig. *5* show crystallization temperature changes over the solidification rate and composition of the ribbons respectively. Obviously, the crystallization temperature does not have significant changes with changing the wheel speed. Therefore, it can be claimed that there is unique crystallisation temperature for the specific composition.
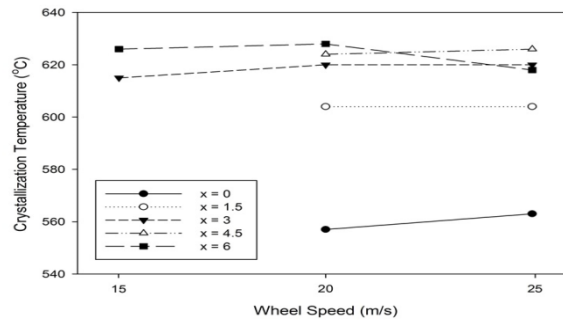
Fig. 4 Crystallization temperature changes over the solidification rate

As it can be derived from
Fig. *5*, the crystallisation temperature moves up to a higher value by a3% increase in Ti and C in the compositions and then will be a steady state. It means that the maximum of non-equilibrium dissolution of Ti and C into the solid phase was 3% and the rest of them lead to formation of TiC precipitates.
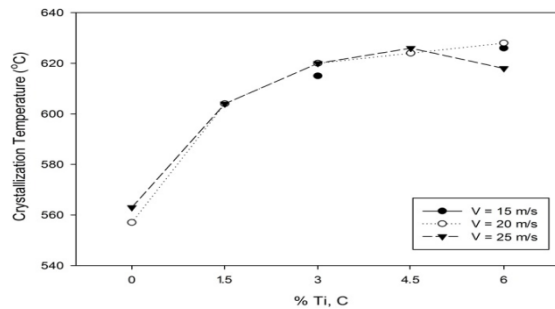

Fig. 5 Crystallization temperature changes over the composition

On the other hand, Good Glass Forming Ability (GFA) is effective on increasing the crystallization temperature. Generally, GFA requires poor crystallization of the super-cooled melt to obtain a glass. Crystallization has to be suppressed down to the glass temperature. Thus, the temperature difference between the melting temperature (T_m) and the glass temperature (T_g) is important [13]. It should be noted that the glass temperature is not fixed and is dependent on different parameters. For example; as the cooling rate is increased, the glass transition temperature is raised. But with constant cooling rate, T_g will increase with increasing Ti and C additions, leading to a higher value of crystallization temperature. The crystallization rates of the ribbons with different wheel speeds are shown in Fig. *6*. It shows that the crystallization rate increases with increasing wheel speed for all the compositions with different effectiveness.
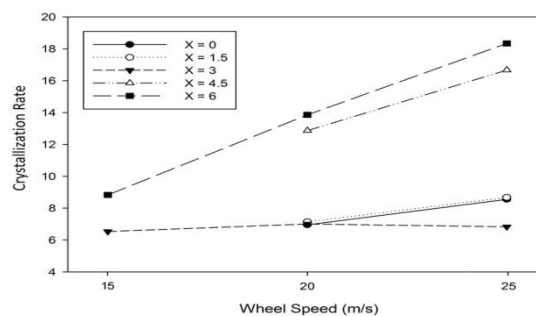

Fig. 6 Crystallization rates of the ribbons with different wheel speeds

This suggests that, increasing the crystallization rate is negligible for the(a) x= 0, (b) x= 1.5 and (c) x= 3 ribbons, while in (e) x= 4.5 and (f) x= 6 ribbons, crystallization rate increase is quite noticeable.Fig. **7**exposes the effect of Ti and C percentage on the crystallization rate clearly. As can be seen, at (h) v=20 and (k) v= 25 m/s of wheel speeds, the crystallization rates of the ribbons increase slightly until 3% of Ti and C, and then they will have a sharp increase.
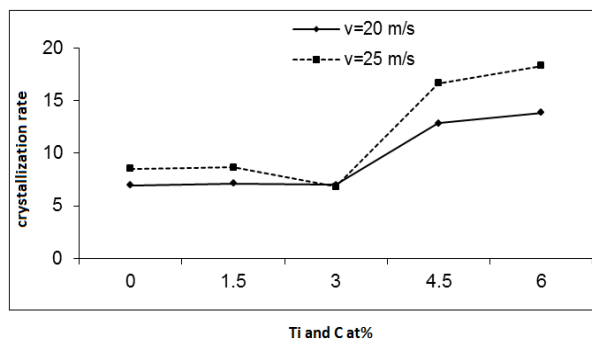

Fig. 7 Crystallization rates of the ribbons with different Ti and C at%

Because the highest possible amount of Ti and C dissolved into the saturated solution of the alloys, extra Ti and C tended to out of the supersaturated solid solution (SSSS) and formed TiC participates [14]. TiC precipitates are the suitable sites for heterogeneous nucleation of crystalline grains from the amorphous phase. These structures have a high energy level, therefore lower activation energy required to reach the equilibrium condition. Thus, crystallization is completed at higher rates.

4. Conclusions

Nanocomposite two-phase $Nd_{9.4}Pr_{0.6}$ $Fe_{77.5-x}B_6Co_6Ga_{0.5}Ti_xC_x$ (a) x=0, (b) x= 1.5, (c) x=3, (e) x= 4.5 and (f) x= 6 ribbons were synthesized from the melt spun method by different solidification rate and were examined by using differential scanning calorimetry (DSC). Thermal measurements of the as-quenched ribbons indicated the crystallization temperature does not have significant changes with changing the wheel speed. Furthermore, DSC measurement shows increasing enhancement of Glass Forming Ability GFA with increasing amounts of TiC addition.

Acknowledgements

References

[1] J Delamare, D Lemarchand, P Vigier, Journal of alloys and compounds **216,** 273 (1995)
[2] D Givord, J Nozieres, J Sánchez Llazamares, F Leccabue, Journal of magnetism and magnetic Materials **111,** 164 (1992).
[3] J J Croat, J F Herbst, R W Lee, F E Pinkerton, Journal of Applied Physics **55,** 2078 (1984).
[4] M Sagawa, S Fujimura, NTogawa, H Yamamoto, Y Matsuura, Journal of Applied Physics **55,** 2083 (1984).
[5] R Lee, E Brewer, NSchaffel, Magnetics IEEE Transactions on **21,** 1958 (1985)
[6] N Talijan, T Zak, J Stajić-Trosić, V Menushenkov, Journal of magnetism and magnetic

materials **258,** 577 (2003).

[7] V Neu, P Crespo, R Schäfer, J Eckert, L Schultz, Journal of magnetism and magnetic materials **157,** 61 (1996).

[8] L.A Dobrzański, MDrakJ. Mater. Process Tech **175,** 149 (2006).

[9] P CampbellPermanent magnet materials and their application(Cambridge University Press) (1996).

[10] R Sabbaghizadeh, M Hashim, S Moraddeh, Electronic Materials Letters **9,** 337 (2013).

[11] R Sabbaghizadeh, M Hashim, G. Bahmanrokh, M Shafie, Journal of Nanoelectronics and Optoelectronics **8,** 302 (2013).

[12] H Chiriac, N Lupu, Physica B: Condensed Matter **299,** 293 (2001).

[13] D Branagan, R McCallum, Journal of alloys and compounds **244,** 40 (1996)

[14] D Branagan, R McCallum, Journal of alloys and compounds **218,** 143 (1995).